|337

Facile Preparation of Bimetallic MOF-derived Supported Tungstophosphoric Acid Composites for Biodiesel Production

Qiuyun Zhang[1,2,3*], Linmin Luo[1], Jiaxing Jin[1], Yaping Wu[1], Yutao Zhang[1,2,3**]

[1] School of Chemistry and Chemical Engineering, Anshun University, 25 College Road, Anshun 561000, Guizhou, China
[2] College Rural Revitalization Research Center of Guizhou, Anshun University, 25 College Road, Anshun 561000, Guizhou, China
[3] Engineering Technology Center of Control and Remediation of Soil Contamination of Guizhou Science and Technology
  Department, Anshun University, 25 College Road, Anshun 561000, Guizhou, China
* First corresponding author, e-mail: sci_qyzhang@126.com; ** Second corresponding author, e-mail: zyt0516@126.com

Abstract

In this work, the novel TPA@C-NiZr-MOF catalyst is synthesized by the impregnation of tungstophosphoric acid (TPA) on the NiZr-based metal-organic framework (NiZr-MOF) followed by calcination up to 300 °C. The as-prepared catalyst materials were structurally, morphologically, and texturally characterized by XRD, FTIR, temperature programmed desorption of NH_3 (TPD-NH_3), N_2 physisorption, SEM, TEM, and XPS. The prepared catalyst can be used as an efficient heterogeneous catalyst for biodiesel production from oleic acid (OA) with methanol. The results indicated that, in comparison to TPA@NiZr-MOF, the TPA@C-NiZr-MOF catalyst calcined at 300 °C exhibits excellent catalytic performance probably owing to the synergistic effect between TPA and metal oxide skeletons, high acidity, as well as larger surface area and pore size. Additionally, the TPA@C-NiZr-MOF catalyst can be reused in up to six cycles with an acceptable conversion. This study showed that the bimetallic MOF-derived composite materials can be used as an alternative potential heterogeneous catalyst toward biorefinery applications.

Keywords

tungstophosphoric acid, NiZr-MOF, esterification, biodiesel

1 Introduction

Energy sources like fossil energy are an essential factor in the twenty-first century. However, these resources are limited due to the depletion of fossil fuel resources and the massive utilization of fossil energy leads to increased environmental concerns [1, 2]. Then, biodiesel (fatty acid methyl esters, FAME) has been recognized as an appropriate alternative to fossil fuel owing to their renewability, biodegradability, and low emission profiles [3, 4]. In general, biodiesel is derived by esterification/transesterification of free fatty acids (FFAs), plant oils, animal fats, waste cooking oils, and microalgae and triglyceride with short-chain alcohols in the presence of homogeneous/heterogeneous catalysts [5]. Although the usage of homogeneous catalysts can achieve a high percentage of conversion rates, it also causes some salient problems such as expensive separation stages and large amounts of chemical wastewater [6]. Therefore, heterogeneous catalysts have just been developed for various applications due to their less hazardous, ease of separation, and recyclability [7–9].

Currently, keggin-type heteropolyacids like tungstophosphoric acid (TPA) are widely used for various acid-catalyzed reactions [10]. Unfortunately, the low surface area and the solubility nature of heteropolyacids in polar solvents make them less useful [11, 12]. Thus, the use of porous oxide materials with acidic character that would provide large specific surface area and pores for incorporation of heteropolyacids and enhance catalytic activity has been suggested.

Metal-organic framework (MOF) is porous coordination materials with attractive properties, including regulatable pore size, large surface areas, and highly ordered architectures [13, 14]. In literature, it has been studied that MOF/bimetallic MOF can be converted to relatively stable metal oxide materials with maintaining the porosity of original MOF through thermal transition process [15–18]. However, there are few attempts to use bimetallic MOF-derived mixed metal oxides supported heteropolyacids for biodiesel production. On this basis, in this work, TPA impregnated

on NiZr-based metal-organic framework (NiZr-MOF) derivates (TPA@C-NiZr-MOF) was prepared and used to synthesize biodiesel from oleic acid. The obtained catalyst was characterized by using different methods to investigate the physical and chemical properties. Moreover, various esterification reaction parameters were optimized. Finally, the stability of as-prepared catalyst was also researched in detail. This study may provide new insights into the design and synthesis of bimetallic MOF-derived composites for biorefinery in industries.

2 Materials and methods

2.1 Chemicals
The chemicals of nickel (II) nitrate hexahydrate ($Ni(NO_3)_2 \cdot 6H_2O$, AR), Zirconium (IV) chloride ($ZrCl_4$, AR), Nickel nitrate hexahydrate ($Ni(NO_3)_2 \cdot 6H_2O$, AR), tungstophosphoric acid ($H_3PW_{12}O_{40} \cdot nH_2O$, TPA, AR), terephthalic acid (H_2-BDC, AR), and oleic acid (C18:1, OA, AR) are commercially available and used without further purification. Deionized water was used in all the experiments.

2.2 Catalyst preparation
TPA@C-NiZr-MOF was prepared by hydrothermal synthesis followed by calcination at 300 °C based on previous literature [19]. Typically, $Ni(NO_3)_2 \cdot 6H_2O$ (0.5 mmol, 0.145 g) and $ZrCl_4$ (0.5 mmol, 0.117 g) were dissolved into 18 ml of N, N-dimethylformamide (DMF), and then TPA (0.40 g) and H_2-BDC (1.5 mmol, 0.249 g) was added and stirred for 60 min. Then, it was transferred to a 25 mL polytetrafluoroethylene-lined reaction kettle at 150 °C for 6 h. Once the reaction kettle had cooled, the resultant slurry was filtered, washed with water and DMF, dried overnight at 60 °C, and marked as TPA@NiZr-MOF precursor. Subsequently, the obtained TPA@NiZr-MOF was calcined at 300 °C for 180 min in air, and the heating rate was 5 °C/min. The obtained composite catalyst was denoted as TPA@C-NiZr-MOF, and these procedures are displayed in Fig. 1. Similarly, NiZr-MOF was synthesized by following the same procedure without the use of TPA.

2.3 Characterization
Wide-angle X-ray diffraction (XRD) was performed using a Bruker D8 Advance with Cu-Kα (1.5406 Å) radiation source. Fourier transform infrared (FTIR) spectra were measured using a PerkinElmer spectrum100 spectrometer using KBr pellets in 400–4000 cm^{-1}. The morphological images were probed by the scanning electron microscope (SEM, Hitachi S4800) at 15 kV and transmission electron
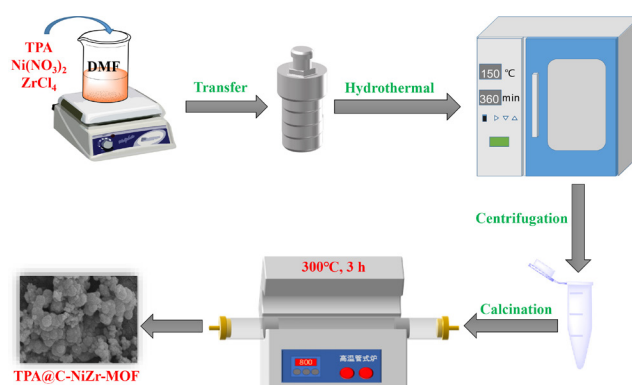

Fig. 1 Schematic illustration of the synthesis process for the TPA@C-NiZr-MOF

microscope (TEM, FEI Tecnai G2 20) at an accelerating voltage of 200 kV. N_2 physisorption measurements were taken on a Quadrasorb EVO instrument (Quantachrome, USA), and the catalyst was ventilated at 150 °C for 12 h before the measurements. The acidity of the catalysts was measured by temperature programmed desorption of NH_3 (TPD-NH_3) using an Auto TP-5080B instrument, the analysis is carried out from 50 to 750 °C at a heating rate of 10 °C/min in the flow of He. X-ray photoelectron spectra (XPS) were carried out on an Thermo ESCALAB 250XI X-ray photoelectron spectrometer.

2.4 Reaction procedure
The catalytic esterification of OA with methanol was performed in a sealed Teflon autoclave (autogenous pressure, 1.0–1.2 MPa) containing 3 g of OA, a certain amount of methanol (methanol:OA molar ratio from 5:1 to 30:1), and TPA@C-NiZr-MOF catalyst (0.03–0.27 g) at 140 °C with magnetic stirring for a desired time (1–5 h). After the completion of reaction, the reaction mixtures are transferred in centrifuge to separate the catalyst. Next, the liquid mixture was further purified for water and excess methanol removal. The acid value of the product was tested according to the ISO 660:2020 standard [20], and the OA conversion was calculated to use up below equation:
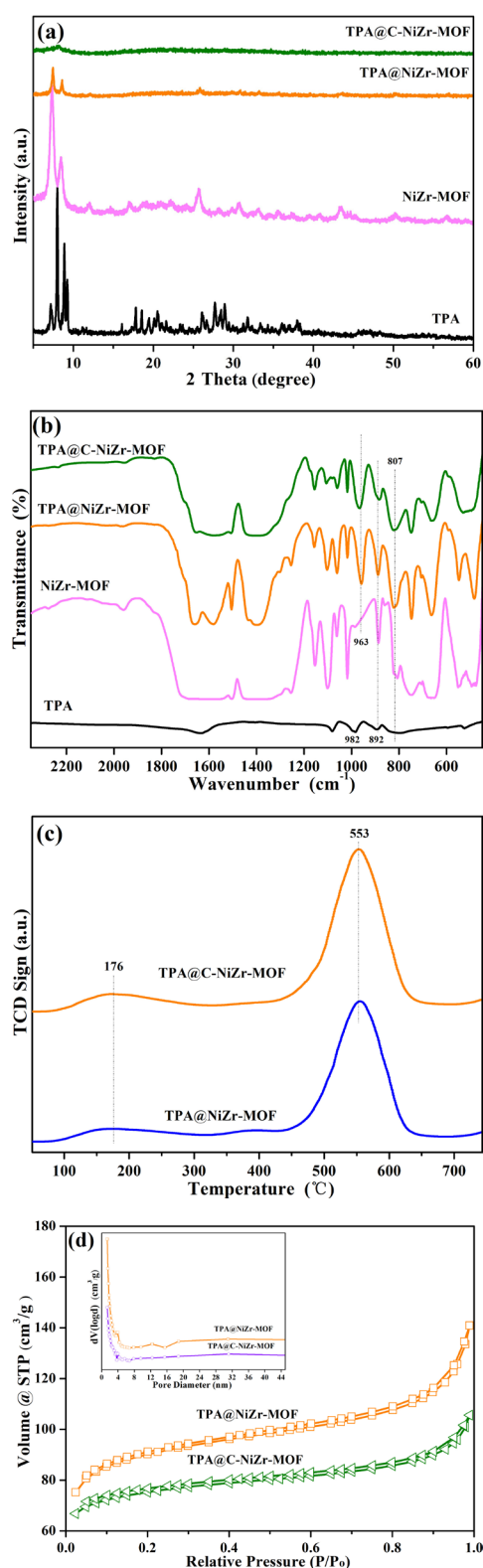
$$\text{Conversion } (\%) = \left[\left(A_0 - A_f \right) / A_0 \right] \times 100\%,$$

where A_0 is the acid value before reaction and A_f is the acid value after reaction.

3 Results and discussion

3.1 Catalyst characterization
The X-ray diffraction patterns of TPA, NiZr-MOF, TPA@NiZr-MOF, and TPA@C-NiZr-MOF catalysts are given in Fig. 2 (a). From the XRD pattern, the diffraction peaks of the

Fig. 2 (a) XRD patterns of TPA, NiZr-MOF, TPA@NiZr-MOF, TPA@C-NiZr-MOF catalysts; (b) FTIR spectra of TPA, NiZr-MOF, TPA@NiZr-MOF, TPA@C-NiZr-MOF catalysts; (c) TPD-NH$_3$ profiles of TPA@NiZr-MOF and TPA@C-NiZr-MOF catalysts; (d) N$_2$ adsorption/desorption isotherm curves of TPA@NiZr-MOF and TPA@C-NiZr-MOF catalysts, the inset is the pore size distributions

parent TPA matched well with the JCPDS database of TPA (No. 50-1857) [21]. For NiZr-MOF, the peaks at 7.4°, 8.4°, and 25.7° were matched well with the characteristic peaks of Zr-MOF [22], suggesting that the structure of NiZr-MOF may be similar to that of Zr-MOF. Moreover, two weak diffraction peaks at 14.6° and 16.9° can be indexed to (010) and (020) planes of Ni-MOF [23]. With TPA being introduced into NiZr-MOF, it exhibits a similar XRD pattern compared with NiZr-MOF although the intensity of the major diffraction peaks decreased, which verified that the introduction of TPA did not influence the structural change of NiZr-MOF. Moreover, the major diffraction peaks of TPA could not be observed from TPA@NiZr-MOF, which was due to the uniform distribution of TPA. After the calcination, in the pattern of TPA@C-NiZr-MOF, the peak at 8.1° and the weak broad peaks at 15–30° can be observed, and other characteristic diffraction peaks of NiZr-MOF cannot be detected, which was probably due to the decomposition of the NiZr-MOF to bimetallic oxides.

The FTIR spectrum of as-prepared catalysts is shown in Fig. 2 (b). Peaks at 982 cm^{-1}, 892 cm^{-1}, and 807 cm^{-1} could be attributed to the Keggin structure (PW$_{12}$O$_{40}^{3-}$) [24]. In addition, it is interesting to note that, a similar FTIR pattern is observed for NiZr-MOF, TPA@NiZr-MOF, and TPA@C-NiZr-MOF, suggesting that these catalysts have the same layered topology. Obviously, the intensities of the NiZr-MOF peaks are considerably decreased for TPA@C-NiZr-MOF, implying that organic ligands have been decomposed after the thermal transition process, the same as previous reports [25]. Moreover, in the spectrum of TPA@C-NiZr-MOF, only one broad peak appeared at 450–550 cm^{-1}, which confirmed the formation of metal oxides. Interestingly, it should be noted that the characteristic absorption peak of TPA (982 cm^{-1}) in Ni-Zn MOF shifts to lower values, implying the existence of the interaction between TPA and metal oxide skeletons. Therefore, the above results clearly showed that the TPA@C-NiZr-MOF hybrids have been successfully prepared.

Also, TPD-NH$_3$ was performed for the acidic property of as-obtained TPA@NiZr-MOF and TPA@C-NiZr-MOF catalysts, and the results are illustrated in Fig. 2 (c). From the TPD-NH$_3$ profiles, both catalysts revealed that two desorption peaks at 176 °C and 553 °C, referring weak and strong acid sites, respectively [26]. Meanwhile, the weak acid sites are associated with the center of metal ions and the strong acid sites are associated with the TPA groups. More importantly, the total acidity of the TPA@C-NiZr-MOF catalyst (8.82 mmol/g) was better

than TPA@NiZr-MOF catalyst (7.52 mmol/g), showing that there was a synergistic effect between TPA and metal oxide skeletons after pyrolysis, which could lead to the enhancement of the esterification.

N_2 physisorption isotherms and pore size distributions for TPA@NiZr-MOF and TPA@NiZr-MOF calcined at 300 °C are shown in Fig. 2 (d). According to the IUPAC classification, the materials all exhibited transient between types II and IV isotherms, indicating mesoporous characteristics [27]. Moreover, TPA@NiZr-MOF had a high BET surface area (S_{BET}) of 441 m^2/g, and the total pore volume (V_{total}) and average pore diameter were measured to be 0.30 cm^3/g and 2.72 nm, respectively. N_2 physisorption calculation was conducted by a Quadrasorb EVO instrument (Quantachrome, USA), and N_2 physisorption calculation come from the Trina Scientific Research Cooperation Center. After calcination, the S_{BET} and V_{total} of the TPA@C-NiZr-MOF catalyst (233 m^2/g and 0.16 cm^3/g) were reduced due to the NiZr-MOF structure shrinking and collapsing. Additionally, the corresponding average pore diameter of TPA@C-NiZr-MOF (2.80 nm) was shown to increase to some extent, which was possibly because the impregnation of TPA could lead to the slight expansion of the pore diameter. From this data, the prepared TPA@C-NiZr-MOF catalyst still retained the mesoporous structure and occupied high S_{BET}, resulting in increased rates of esterification.

The surface morphologies of TPA@NiZr-MOF and TPA@C-NiZr-MOF catalysts were studied by SEM and TEM images and have been displayed in Fig. 3 and Fig. 4. As observed in Fig. 3 (a), (b), the TPA@NiZr-MOF shows many spherical shape structures with the size of about
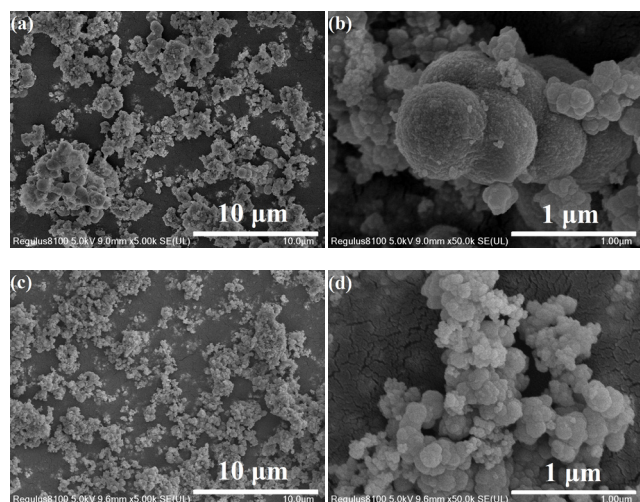
Fig. 3 SEM images of TPA@NiZr-MOF ((a) scale bar: 10 μm, (b) scale bar: 1 μm) and TPA@C-NiZr-MOF ((c) scale bar: 10 μm, (d) scale bar: 1 μm) catalysts
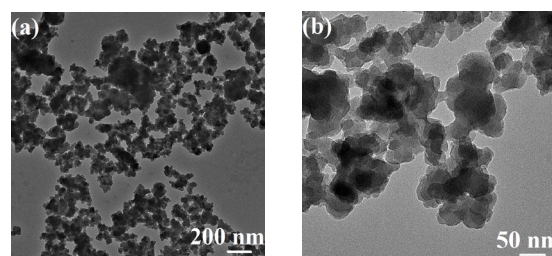
Fig. 4 TEM images of TPA@C-NiZr-MOF catalyst ((a) scale bar: 200 nm, (b) scale bar: 50 nm)

500 nm with the agglomeration of the particle due to their high S_{BET}. Interestingly, the morphology of the TPA@C-NiZr-MOF was maintained that of the TPA@NiZr-MOF (Fig. 3 (c), (d)), suggesting that the basic morphology of the TPA@NiZr-MOF would not be affected by thermal treatment. However, in TPA@C-NiZr-MOF, an obvious decrease in particle size was observed due to the shrinkage of the NiZr-MOF framework. Additionally, as depicted in Fig. 4 (a), (b), it is clearly observed from TEM images that TPA@C-NiZr-MOF presents a spherical shape with relatively uniformly sized particles, and it is also observed that the generation of many pores due to the accumulation of particles, resulting in provided the available active sites for the catalytic reaction [28], and these results were consistent with those observed from SEM analysis.

XPS was employed to analyze the chemical state of as-obtained TPA@C-NiZr-MOF (Fig. 5). As shown in Fig. 5 (a), the peak observed at 182.6 eV and 184.9 eV supports the presence of Zr^{4+} in TPA@C-NiZr-MOF catalyst corresponding to Zr 3d state [29]. It can be seen from Fig. 5 (b) that the peak at 874.1 eV and 856.2 eV refers to Ni 2$p_{1/2}$ and Ni 2$p_{3/2}$ states, respectively. Moreover, the satellite signals at 880.0 eV and 861.0 eV were also observed [30]. Fig. 5 (c) shows the XPS spectrum of W 4f. The peaks with binding energies at 37.8 eV and 35.8 eV are attributed to W 4$f_{5/2}$ and W 4$f_{7/2}$ of W^{6+} in TPA [31]. Surprisingly, an additional weak energy peak appeared at 29–33 eV, which was probably due to the partial decomposition of TPA leading to the formation of a lower chemical valence [32]. This demonstrated that the introduced TPA groups have been loading on the framework, in agreement with XRD and FTIR results.

3.2 Catalytic performance of different catalysts
The esterification was evaluated with the prepared TPA@NiZr-MOF and TPA@C-NiZr-MOF catalysts. As shown in Fig. 6, the higher conversion of OA on TPA@C-NiZr-MOF than on TPA@NiZr-MOF (95.7% versus 41.1%) at 140 °C for 5 h, and this is likely to be
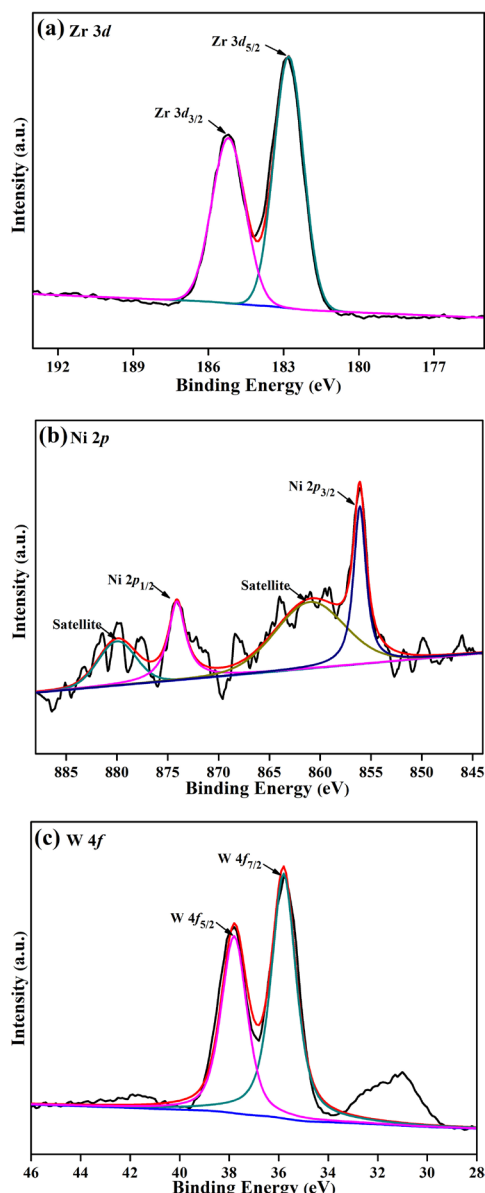
Fig. 5 XPS spectrum of prepared TPA@C-NiZr-MOF catalyst (a) Zr 3*d* spectra, (b) Ni 2*p* spectra, (c) W 4*f* spectra
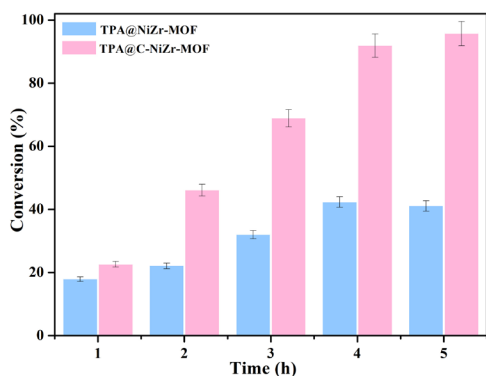

Fig. 6 The catalytic performance of TPA@NiZr-MOF and TPA@C-NiZr-MOF catalysts for esterification. Reaction conditions: Methanol/OA = 20/1, Temperature = 140 °C, Catalyst amount = 0.15 g

attributed to TPA@C-NiZr-MOF has a larger pore size and high acidity (calculated by TPD-NH$_3$ results). Hence, TPA@C-NiZr-MOF was used in the subsequent study.

3.3 Effects of various parameters on the esterification

Reaction time and temperature influence were analyzed by fixing the TPA@C-NiZr-MOF catalyst, and the results are shown in Fig. 7 (a). It can be seen that the conversion of OA rose with temperature, and the reaction conversion was optimal at 140 °C, moreover, the oleic acid conversion of 98% was obtained using MoO$_3$/B-ZSM-5 catalyst with temperature of 160 °C [33], suggesting that the
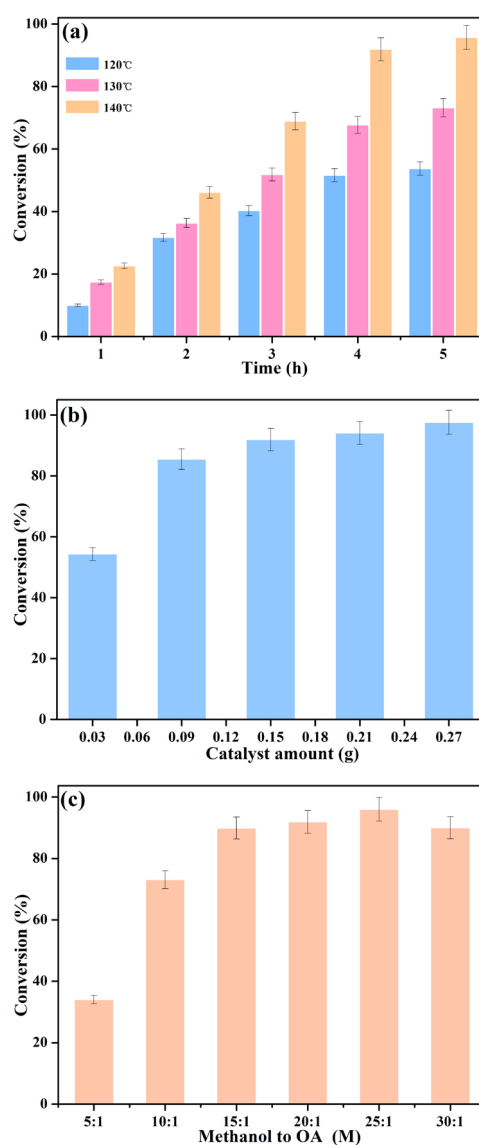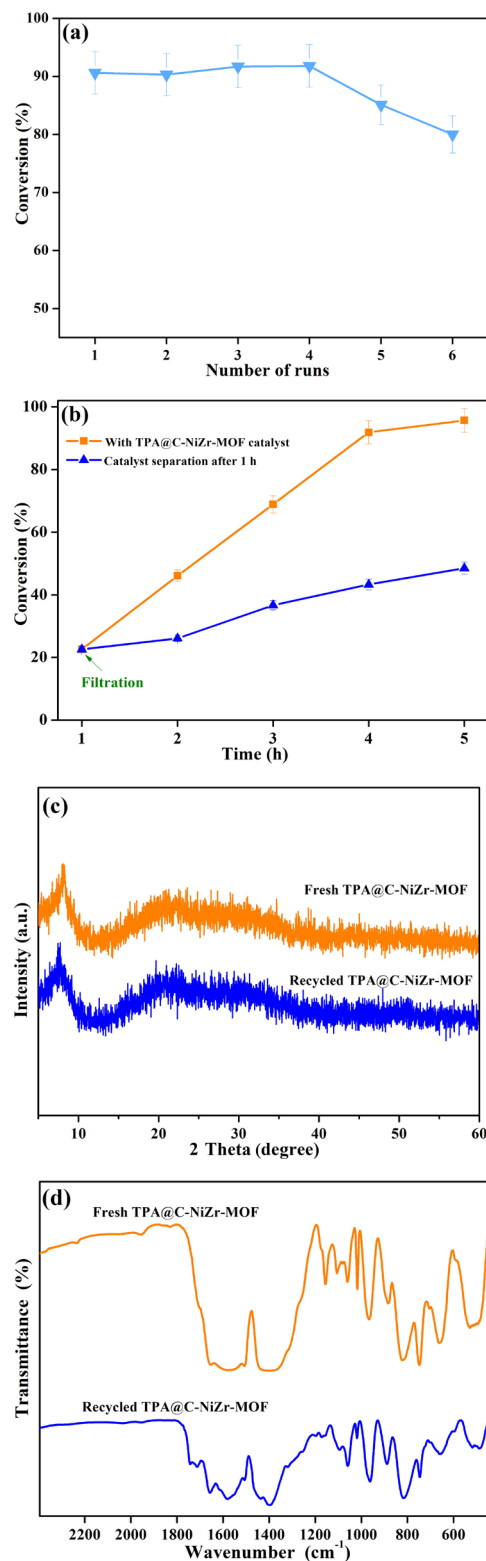

Fig. 7 Influence of (a) reaction time and temperature (Reaction conditions: Methanol/OA = 20/1, Catalyst amount = 0.15 g), (b) catalyst amount (Reaction conditions: Methanol/OA = 20/1, Temperature = 140 °C, Time = 4 h), and (c) Methanol:OA molar ratio (Reaction conditions: Temperature = 140 °C, Time = 4 h, Catalyst amount = 0.15 g)

temperature in this work are relatively lower than or comparable to previous studies. Similarly, the OA conversion rose with time, however, the conversion stayed almost constant after 4 h due to the reversible esterification reaction. Accordingly, the favorable reaction time and temperature were found to be 4 h and 140 °C, respectively.

The influence of catalyst amount on OA conversion was also estimated. As exhibited in Fig. 7 (b), when a low amount of the catalyst (0.03 g) was applied, the OA conversion was attained only at 54.3%, this might be ascribed to few available acidic sites within the reaction system. However, the OA conversion was increased from 54.3% to 91.9% by increase in loading of catalyst from 0.03 g to 0.15 g. Moreover, further increase in amount of catalyst does not significantly affect the conversion, which is probably due to too high catalyst amount would make the reactant mixture more viscous [34]. By drawing on the results, the optimum catalyst amount was considered to be 0.15 g. Additionally, the effect of methanol:OA molar ratio from 5:1 to 30:1 on the OA conversion is shown in Fig. 7 (c). The OA conversion increases with the molar ratio methanol:OA from 5:1 to 20:1. But, the conversion decreased with further increasing the methanol:OA molar ratio above 25:1 is probably due to excessive methanol leading to a dilution effect in the reaction system [35]. According to these observations, the suitable methanol:OA molar ratio was 20:1.

3.4 Catalyst recycling

Catalyst reusability is an important parameter for heterogeneous catalysis. Thus, the recyclability of TPA@C-NiZr-MOF was assessed under the above optimal conditions. After each cycle, the TPA@C-NiZr-MOF was recovered by centrifugation, after which directly reused for the next reaction cycle. According to Fig. 8 (a), it can be seen that the TPA@C-NiZr-MOF catalyst demonstrated appreciable catalytic activity in its reutilization for esterification, and the OA conversion close to 80% could still be reached at the sixth cycle. Besides, the hot filtration experiment is also presented in Fig. 8 (b). It was noticed that the conversion of OA was not significantly increased after the removal of the catalyst, indicating the heterogeneous character of the catalyst. Whereas, the slight increase in conversion might be due to a low leaching of the TPA active phase. Interestingly, the analysis of the XRD and FTIR spectrum (Fig. 8 (c), (d)) revealed that the characteristic peaks of the TPA@C-NiZr-MOF catalyst before and after esterification still exist, suggesting the good structural stability of the catalyst. Based on the above results, the reduction in the

Fig. 8 (a) Recyclability of TPA@C-NiZr-MOF for the esterification, reaction conditions: Methanol/OA = 20/1, Temperature = 140 °C, Time = 4 h, Catalyst amount = 0.15 g; (b) the hot filtration test of TPA@C-NiZr-MOF, reaction conditions: Methanol/OA = 20/1, Temperature = 140 °C, Catalyst amount = 0.15 g; (c) XRD patterns of the fresh and spent TPA@C-NiZr-MOF after the sixth cycle; (d) FTIR spectra of the fresh and spent TPA@C-NiZr-MOF after the sixth cycle.

OA conversion might be attributed to the leaching of part of active species during the transfer between reaction runs, and the deposition of reaction substrates and product intermediate on the active site of the catalyst [36].

4 Conclusion

In summary, the TPA loaded on NiZr-MOF-derived bimetal oxide was successfully synthesized, and the bimetallic MOF-derived TPA@C-NiZr-MOF show excellent activity and durability for catalyzing esterification of OA with methanol because of their high acidity, larger BET surface area and pore size, and the synergy between TPA and metal oxide skeletons. Under the optimized conditions of methanol to OA molar ratio (20:1), catalyst amount of 0.15 g, 140 °C for 4 h, the OA conversion was 91.9%. Noticeably, the TPA@C-NiZr-MOF showed good

catalytic stability with an acceptable conversion. This study provides the novel bimetallic MOF-derived composite with good activity and suitable reusability, which may find useful applications for the green production of biofuels in the industry.

References

[1] Devarajan, Y., Munuswamy, D. B., Subbiah, G., Vellaiyan, S., Nagappan, B., Varuvel, E. G., Thangaraja, J. "Inedible oil feedstocks for biodiesel production: A review of production technologies and physicochemical properties", Sustainable Chemistry and Pharmacy, 30, 100840, 2022.
https://doi.org/10.1016/j.scp.2022.100840

[2] Pan, H., Xia, Q., Wang, Y., Shen, Z., Huang, H., Ge, Z., Li, X., He, J., Wang, X., Li, L., Wang, Y. "Recent advances in biodiesel production using functional carbon materials as acid/base catalysts", Fuel Processing Technology, 237, 107421, 2022.
https://doi.org/10.1016/j.fuproc.2022.107421

[3] Zhang, Q., Yang, B., Tian, Y., Yang, X., Yu, R., Wang, J., Deng, T., Zhang, Y. "Fabrication of silicotungstic acid immobilized on Ce-based MOF and embedded in Zr-based MOF matrix for green fatty acid esterification", Green Processing and Synthesis, 11(1), pp. 184–194, 2022.
https://doi.org/10.1515/gps-2022-0021

[4] Supamathanon, N., Boonserm, K., Osakoo, N., Wittayakun, J., Prayoonpokarach, S., Chanlek, N., Dungkaew, W. "Potassium supported on zeolite-geopolymer hybrid materials as a new solid base catalyst for transesterification of soybean oil", Renewable Energy, 202, pp. 1460–1469, 2023.
https://doi.org/10.1016/j.renene.2022.12.018

[5] Maroju, P. A., Ganesan, R., Ray Dutta, J. "Efficient biodiesel production from rice bran oil using magnetite immobilized-recombinant lipase from probiotic *Bacillus licheniformis*", Green Chemistry, 24(22), pp. 8800–8811, 2022.
https://doi.org/10.1039/D2GC03022E

[6] Zhang, Q., Hu, M., Wang, J., Lei, Y., Wu, Y., Liu, Q., Zhao, Y., Zhang, Y. "Synthesis of silicotungstic acid/Ni-Zr-O composite nanoparticle by using bimetallic Ni-Zr MOF for fatty acid esterification", Catalysts, 13(1), 40, 2023.
https://doi.org/10.3390/catal13010040

[7] Woo, J., Joshi, R., Park, Y.-K., Jeon, J.-K. "Biodiesel production from jatropha seeds with bead-type heterogeneous catalyst", Korean Journal of Chemical Engineering, 38(4), pp. 763–770, 2021.
https://doi.org/10.1007/s11814-021-0759-7

[8] Yusuff, A. S., Thompson-Yusuff, K. A., Porwal, J. "Sulfonated biochar catalyst derived from eucalyptus tree shed bark: synthesis, characterization and its evaluation in oleic acid esterification", RSC Advances, 12(17), pp. 10237–10248, 2022.
https://doi.org/10.1039/D1RA09179D

[9] Sangsiri, P., Laosiripojana, N., Daorattanachai, P. "Synthesis of sulfonated carbon-based catalysts from organosolv lignin and methanesulfonic acid: Its activity toward esterification of stearic acid", Renewable Energy, 193, pp. 113–127, 2022.
https://doi.org/10.1016/j.renene.2022.05.012

[10] Tayebee, R., Lee, A. F., Frattini, L., Rostami, S. "$H_3PW_{12}O_{40}$/SBA-15 for the solventless synthesis of 3-substituted indoles", Catalysts, 9(5), 409, 2019.
https://doi.org/10.3390/catal9050409

[11] Zhang, Q., Lei, D., Luo, Q., Deng, T., Cheng, J., Zhang, Y., Ma, P. "Immobilizing Ni (II)-exchanged heteropolyacids on silica as catalysts for acid-catalyzed esterification reactions", Periodica Polytechnica Chemical Engineering, 65(1), pp. 21–27, 2021.
https://doi.org/10.3311/PPch.14788

[12] Wang, C., Li, A., Ma, Y., Qing, S. "Preparation of formate-free PMA@MOF-808 catalysts for deep oxidative desulfurization of model fuels", Environmental Science and Pollution Research, 29(26), pp. 39427–39440, 2022.
https://doi.org/10.1007/s11356-022-18685-2

[13] Zhang, Y., Wang, B., Wang, R. "Functionally decorated metal-organic frameworks in environmental remediation", Chemical Engineering Journal, 455, 140741, 2023.
https://doi.org/10.1016/j.cej.2022.140741

[14] Zhang, Q., Lei, Y., Li, L., Lei, J., Hu, M., Deng, T., Zhang, Y., Ma, P. "Construction of the novel PMA@Bi-MOF catalyst for effective fatty acid esterification", Sustainable Chemistry and Pharmacy, 33, 101038, 2023.
https://doi.org/10.1016/j.scp.2023.101038

[15] Wu, T.-L., Tan, X.-N., Nong, T.-T., Pan, Y.-J., Qiu, P.-F., He, J.-Q., Zhou, Y., Tan, X.-C., Huang, Z.-Y., Han, L. "Rational synthesis of bimetallic CoFe-MOF-74 grown on Ni foam converted into bamboo-shoot-like α-Co(OH)$_2$/CoFe$_2$O$_4$ nanorods for high-performance supercapacitors", Chemical Engineering Journal, 457, 141238, 2023.
https://doi.org/10.1016/j.cej.2022.141238

[16] Liu, H., Chang, Z., Fu, J., Hou, Z. "A CuZn-BTC derived stable Cu/ZnO@SiO$_2$ catalyst for ethanol dehydrogenation", Applied Catalysis B: Environmental, 324, 122194, 2023.
https://doi.org/10.1016/j.apcatb.2022.122194

[17] Salari, H. "Kinetics and mechanism of enhanced photocatalytic activity under visible light irradiation using Cr$_2$O$_3$/Fe$_2$O$_3$ nanostructure derived from bimetallic metal organic framework", Journal of Environmental Chemical Engineering, 7(3), 103092, 2019.
https://doi.org/10.1016/j.jece.2019.103092

[18] Chen, T., Wang, R., Sun, C., Kong, D., Lu, S., Li, X. "Metal-organic frameworks templated micropore-enriched defective MnCeO$_x$ for low temperature chlorobenzene oxidation", Applied Catalysis A: General, 645, 118845, 2022.
https://doi.org/10.1016/j.apcata.2022.118845

[19] Wang, M., Li, F., Dong, J., Lin, X., Liu, X., Wang, D., Cai, W. "MOF-derived CoCeO$_x$ nanocomposite catalyst with enhanced anti-coking property for ethanol reforming with CO$_2$", Journal of Environmental Chemical Engineering, 10(3), 107892, 2022.
https://doi.org/10.1016/j.jece.2022.107892

[20] ISO "ISO 660:2020 Animal and vegetable fats and oils — Determination of acid value and acidity", International Organization for Standardization, Geneva, Switzerland, 2020.

[21] Negm, N. A., Betiha, M. A., Alhumaimess, M. S., Hassan, H. M. A., Rabie, A. M. "Clean transesterification process for biodiesel production using heterogeneous polymer-heteropoly acid nanocatalyst", Journal of Cleaner Production, 238, 117854, 2019.
https://doi.org/10.1016/j.jclepro.2019.117854

[22] Zhang, Q., Yang, T., Liu, X., Yue, C., Ao, L., Deng, T., Zhang, Y. "Heteropoly acid-encapsulated metal-organic framework as a stable and highly efficient nanocatalyst for esterification reaction", RSC Advances, 9(29), pp. 16357–16365, 2019.
https://doi.org/10.1039/C9RA03209F

[23] Yang, M., Bai, Q. "Flower-like hierarchical Ni-Zn MOF microspheres: Efficient adsorbents for dye removal", Colloids and Surfaces A: Physicochemical and Engineering Aspects, 582, 123795, 2019.
https://doi.org/10.1016/j.colsurfa.2019.123795

[24] Kulkarni, M. G., Gopinath, R., Meher, L. C., Dalai, A. K. "Solid acid catalyzed biodiesel production by simultaneous esterification and transesterification", Green Chemistry, 8(12), pp. 1056–1062, 2006.
https://doi.org/10.1039/B605713F

[25] Rezaee, S., Shahrokhian, S. "Facile synthesis of petal-like NiCo/NiO-CoO/nanoporous carbon composite based on mixed-metallic MOFs and their application for electrocatalytic oxidation of methanol", Applied Catalysis B: Environmental, 244, pp. 802–813, 2019.
https://doi.org/10.1016/j.apcatb.2018.12.013

[26] Ibrahim, S. M., Mustafa, A. "Synthesis and characterization of new bifunctional SnZrSi oxide catalysts for biodiesel production", Journal of Molecular Liquids, 354, 118811, 2022.
https://doi.org/10.1016/j.molliq.2022.118811

[27] Thommes, M., Kaneko, K., Neimark, A. V., Olivier, J. P., Rodriguez-Reinoso, F., Rouquerol, J., Sing, K. S. W. "Physisorption of gases, with special reference to the evaluation of surface area and pore size distribution (IUPAC Technical Report)", Pure and Applied Chemistry, 87(9–10), pp. 1051–1069, 2015.
https://doi.org/10.1515/pac-2014-1117

[28] Krishnamurthy, K. N., Sridhara, S. N., Ananda Kumar, C. S. "Optimization and kinetic study of biodiesel production from *Hydnocarpus wightiana* oil and dairy waste scum using snail shell CaO nano catalyst", Renewable Energy, 146, pp. 280–296, 2020.
https://doi.org/10.1016/j.renene.2019.06.161

[29] Su, Y., Zhang, Z., Liu, H., Wang, Y. "Cd$_{0.2}$Zn$_{0.8}$S@UiO-66-NH$_2$ nanocomposites as efficient and stable visible-light-driven photocatalyst for H$_2$ evolution and CO$_2$ reduction", Applied Catalysis B: Environmental, 200, pp. 448–457, 2017.
https://doi.org/10.1016/j.apcatb.2016.07.032

[30] Wang, M., Wang, C., Zhu, L., Rong, F., He, L., Lou, Y., Zhang, Z. "Bimetallic NiCo metal-organic frameworks for efficient non-Pt methanol electrocatalytic oxidation", Applied Catalysis A: General, 619, 118159, 2021.
https://doi.org/10.1016/j.apcata.2021.118159

[31] Ji, H., Sun, J., Wu, P., Wu, Y., He, J., Cha, Y., Zhu, W., Li, H. "Silicotungstic acid immobilized on lamellar hexagonal boron nitride for oxidative desulfurization of fuel components", Fuel, 213, pp. 12–21, 2018.
https://doi.org/10.1016/j.fuel.2017.08.076

[32] Xu, F., Liu, C., Li, J.-X., Zhan, C.-Z., Xun, Q.-N., Zhang, W.-S., Xing, W.-F., Chang, G.-G. "Hierarchically porous single catalyst Ru/HPW/UiO-66 with synergistic acid/metal sites for one-pot catalytic synthesis of γ-valerolactone", New Journal of Chemistry, 46(27), pp. 13047–13053, 2022.
https://doi.org/10.1039/D2NJ02266D

[33] Mohebbi, S., Rostamizadeh, M., Kahforoushan, D. "Effect of molybdenum promoter on performance of high silica MoO$_3$/B-ZSM-5 nanocatalyst in biodiesel production", Fuel, 266, 117063, 2020.
https://doi.org/10.1016/j.fuel.2020.117063

[34] Alhassana, F. H., Rashid, U., Taufiq-Yap, Y. H. "Ferric-manganese doped sulphated zirconia nanoparticles catalyst for single-step biodiesel production from waste cooking oil: Characterization and optimization", International Journal of Green Energy, 13(13), pp. 1305–1313, 2016.
https://doi.org/10.1080/15435075.2014.966267

[35] Rao, A. V. R. K., Dudhe, P., Chelvam, V. "Role of oxygen defects in basicity of Se doped ZnO nanocatalyst for enhanced triglyceride transesterification in biodiesel production", Catalysis Communications, 149, 106258, 2021.
https://doi.org/10.1016/j.catcom.2020.106258

[36] Falowo, O. A., Ojumu, T. V., Pereao, O., Betiku, E. "Sustainable biodiesel synthesis from honne-rubber-neem oil blend with a novel mesoporous base catalyst synthesized from a mixture of three agrowastes", Catalysts, 10(2), 190, 2020.
https://doi.org/10.3390/catal10020190